Catalysis Science & Technology

ROYAL SOCIETY OF CHEMISTRY

PAPER

View Article Online
View Journal

Cite this: DOI: 10.1039/d0cy00783h

Unraveling the hydrolysis of β-1,4-glycosidic bonds in cello-oligosaccharides over carbon catalysts†

Pengru Chen, [ab] Abhijit Shrotri [*a] and Atsushi Fukuoka [*a]

Received 17th April 2020,
Accepted 16th June 2020

DOI: 10.1039/d0cy00783h

rsc.li/catalysis

Carbon catalysts having weakly acidic groups are uniquely active for hydrolysis of cellulose to produce cello-oligosaccharides and glucose. Although adsorption of cellulose molecules on carbon is considered as the cause for this behavior, the effect of adsorption on the reaction is not well understood. In order to understand the underlying mechanism, we investigated the hydrolysis of cello-oligosaccharides with varying chain lengths over different catalysts. Carbon catalysts favored hydrolysis of larger oligosaccharides with an 11-fold increase in the reaction rate constant from cellobiose to cellohexaose. The activation energy required to cleave the glycosidic bonds was reduced concurrently with the increase in molecule size. Based on these data, in conjugation with the stronger affinity of adsorption for larger oligosaccharides, we propose that axial adsorption within the micropores of carbon causes conformational change in the structure of cello-oligosaccharide molecules, resulting in reduction of activation energy required to cleave the β-1,4-glycosidic bonds. Consequently, this translates to the higher rate of reaction for larger cello-oligosaccharides and explains the high reactivity of carbon catalysts towards cellulose hydrolysis.

Introduction

Cellulose, the primary component of lignocellulosic biomass, is the most abundant carbon-based renewable resource on our planet. It is a biopolymer composed of anhydro-glucose units linked by β-1,4-glycosidic bonds.[1,2] Catalytic hydrolysis of the β-1,4-glycosidic bonds in cellulose is a crucial step in producing biofuels and value-added chemicals, which can reduce the dependence on fossil fuels and the petroleum industry.[3–5]

Enzymes[6–8] and acid catalysts[9–12] are effective for hydrolysis of cellulose to oligosaccharides and glucose. Partial hydrolysis produces water-soluble cello-oligosaccharides as major components,[13,14] which possess repeated β-1,4-glycosidic linkages but have a low degree of polymerization (DP). These oligosaccharides exhibit biological activity that can benefit the growth and health of plants, animals, and humans.[15–17] Complete hydrolysis of cellulose produces glucose, a precursor for value-added chemicals and fuels.[18–21]

Carbon catalysts are the most active for hydrolysis of cellulose among heterogeneous acid catalysts. They are also benign and do not contaminate the product solution, making them ideal for synthesis of cello-oligosaccharides for use in agriculture and healthcare industries.[9,22,23] Carbon catalysts bearing weakly acidic functional groups such as hydroxyl (–OH) and carboxylic (–COOH) groups show comparatively high activity along with good hydrothermal stablity.[24,25] Owing to the insoluble nature of cellulose, a strong interaction between the catalyst and cellulose is essential in a heterogeneous reaction. The polyaromatic surface of a carbon catalyst can adsorb cellulose molecules by CH–π and hydrophobic interactions,[26] and it is believed that this adsorption promotes the interaction between acidic functional groups and β-1,4-glycosidic bonds.[5] The DP of the adsorbed molecules can affect their adsorption capacity and larger oligosaccharides show higher affinity towards the carbon surface.[26–28] Katz's group found that there was a monotonic decrease in the free energy of adsorption with an increase in the chain length of oligosaccharides over mesoporous carbon nanoparticles.[28] Our group observed a linear decrease in the adsorption enthalpy with an increase in the chain length of oligosaccharides.[26]

The change in adsorption affinity with the chain length of oligosaccharides can affect the selectivity for cello-oligosaccharides produced during cellulose hydrolysis. In a previous study, we found that carbon can catalyze the hydrolysis of cellulose in a semi-flow reactor to yield cello-oligosaccharides without forming large amounts of glucose.

[a] Institute for Catalysis, Hokkaido University, Kita 21 Nishi 10, Kita-ku, Sapporo, Hokkaido 001-0021, Japan. E-mail: ashrotri@cat.hokudai.ac.jp, fukuoka@cat.hokudai.ac.jp
[b] Graduate School of Chemical Sciences and Engineering, Hokkaido University, Kita 13 Nishi 8, Kita-ku, Sapporo, Hokkaido 060-8628, Japan

† Electronic supplementary information (ESI) available. See DOI: 10.1039/d0cy00783h

The distribution of DP, determined by quantitative MALDI-TOF MS analysis, suggested a decrease in the rate of hydrolysis as the reaction progressed.[29] However, there is a lack of holistic understanding about the dependence of molecule size on the rate of hydrolysis and the influence of adsorption during the reaction. Therefore, a fundamental approach towards assessing the change in the rate of hydrolysis from a kinetic and mechanistic perspective is essential to determine the underlying factors responsible for the high activity of carbon catalysts.

In this study, we report the hydrolysis of a series of cello-oligosaccharides in the presence of heterogeneous and homogeneous catalysts. Kinetic analysis is done to compare the change in the rate of hydrolysis over different catalysts. Investigation on the adsorption affinity of oligosaccharides along with determination of apparent activation energy is conducted to ascertain the factors responsible for the change in the hydrolysis rate. Based on the experimental results, we propose a plausible mechanism which explains the hydrolysis behavior of large cellulose molecules over carbon catalysts.

Experimental section

Materials

Activated carbon (denoted as AC) was supplied from Ajinomoto Fine-Techno (volume mean diameter = 42 μm). Amberlyst 70 (0.4–0.8 mm) was purchased from Organo Corporation. H-Beta was supplied from Catalysis Society of Japan. Cellotriose (G3, 95%), cellotetraose (G4, 95%), cellopentaose (G5, 95%) and cellohexaose (G6, 94%) were purchased from Megazyme. Glucose and cellobiose were purchased from Kanto Chemical Industries. 1,6-Hexanediol and sulfuric acid (H_2SO_4, 98%) were purchased from Wako Pure Chemical Industries. DMSO was obtained from Tokyo Chemical Industry.

Air oxidation of carbon catalysts

Air oxidation of carbon was performed using a method reported previously.[29] Briefly, activated carbon AC (4.0 g) was spread on a Pyrex dish of diameter 130 mm with a uniform thickness. The sample was then heated in a muffle furnace in air with the following temperature program: 298 to 393 K at a rate of 10 K min^{-1}, and then maintained at 393 K for 2 h to remove the physisorbed water, followed by heating to 698 K at a rate of 4 K min^{-1} and then maintaining at 698 K for further 10 h. The oxidized carbon catalyst was denoted as AC-air. AC-air-L was prepared *via* the same method except for lowering the oxidation temperature to 673 K.

Characterization of catalysts

The specific surface area of the solid catalysts was determined by N_2 adsorption–desorption measurement (BEL Japan, BELSORP-mini) after vacuum drying at 393 K for 3 h. The total amount of acidic functional groups on the solid catalysts was calculated by titration.[30] The acidity of H-beta catalyst was also quantified by NH_3-temprature programmed desorption (TPD) (BEL Japan, BELCAT-A coupled with a mass spectrometer).

Catalytic reactions

Hydrolysis of cello-oligosaccharides was performed in a glass tube placed inside a pressure-resistant hastelloy reactor (5 mL, TVS-1). For a typical reaction, 0.5 mL of water containing 1 μmol of cello-oligosaccharide substrate was added to the glass tube with 5 mg of solid catalyst (in the case of H_2SO_4, 6.4 μmol of acid was used to replicate the acid content of 5 mg of AC-air) and a magnetic stirrer bar. The glass tube was then placed in the reactor. The setup was purged and then pressurized to 0.5 MPa with argon (Ar) before immersing it into a heated oil bath for a set period of time. After the reaction, the reactor was cooled to room temperature and 0.1 mL of water containing 1 μmol of 1,6-hexanediol was added to the mixture to serve as an internal standard. The catalyst was separated from the reaction mixture by centrifugation and then washed three times with DMSO (1 mL) to extract adsorbed sugar molecules. The reaction solution and the liquids obtained after washing were mixed and diluted to 5 mL using a volumetric flask. The obtained solution was analyzed to calculate the concentration of oligosaccharides by using a high-performance liquid chromatography (HPLC) system equipped with a refractive index detector (Shimadzu LC 10-ATVP) and a series of three Shodex Sugar SB 802.5HQ columns (ø 8 × 300 mm; eluent, water 0.5 mL min^{-1}; 328 K).

Adsorption of cello-oligosaccharides

Adsorption of oligosaccharides on the solid catalysts was performed at room temperature. A solid catalyst (5 mg) was added to a vial containing a 0.5 mL aqueous solution of adsorbate. The mixture was equilibrated under stirring for a period of 30 min which was sufficient to reach the adsorption equilibrium (Fig. S1†). The sample was subsequently filtered, and the solution was analyzed using the HPLC system described above. The amount of substrate adsorbed was calculated as the difference between the sugar concentrations in the liquid phase before and after adsorption.

Results and discussion

Characterization of catalysts

Carbon catalysts containing weakly acidic functional groups were prepared by air-oxidation of activated carbon (named AC) at elevated temperature. Amberlyst 70 (sulfonated resin catalyst), H-beta zeolite and homogeneous H_2SO_4 were used for comparing the activity with carbon materials. The N_2-adsorption isotherms for the solid catalysts are shown in Fig. S2.† The Brunauer–Emmett–Teller (BET) surface area of the carbon catalyst prepared by oxidation at 698 K (named AC-air, burn-off 53 %) was calculated to be 877 m^2 g^{-1}, which was lower than that of pristine AC (1143 m^2 g^{-1}) owing to the collapse of some pores during the oxidation treatment

Table 1 BET surface area and number of acid sites on the solid acid catalysts

Catalyst	BET surface area ($m^2\ g^{-1}$)	Total number of acid sites ($\mu mol\ g^{-1}$)
AC	1143	355
AC-air-L	1214	2075
AC-air	877	2560
Amberlyst 70	—	3172
H-Beta zeolite	607	296

(Table 1). AC-air-L, a catalyst prepared by oxidation under milder conditions (673 K, burn-off 30%), exhibited a similar surface area (1214 $m^2\ g^{-1}$) to AC because of its lower degree of oxidation. Zeolite H-beta had a surface area of 607 $m^2\ g^{-1}$, a value typical for zeolite catalysts. The N_2 adsorption over Amberlyst 70 was negligible as the resin catalyst is not porous. However, the resin is permeable to reactants in aqueous solution, allowing access to the acid sites.[31] The number of acidic functional groups on the catalysts was calculated by titration with NaOH.[30] Amberlyst 70 showed the highest number of acid functional groups (3172 $\mu mol\ g^{-1}$) originating from $-SO_3H$ groups. Acidic sites originating from carboxyl, hydroxyl and lactone groups are known to be present over oxidized carbon catalysts.[25] The total number of acidic functional groups in AC-air and AC-air-L was determined to be 2560 $\mu mol\ g^{-1}$ and 2075 $\mu mol\ g^{-1}$, respectively. The lower oxidation temperature of AC-air-L (673 K) introduced fewer functional groups as expected. Titration of H-beta showed a low concentration of acid sites of 296 $\mu mol\ g^{-1}$, consistent with the value (299 $\mu mol\ g^{-1}$) quantified using NH_3-TPD.

Cello-oligosaccharide hydrolysis

Hydrolysis of cello-oligosaccharides with a DP ranging from 2–6 was performed in the presence of AC-air at 413 K to investigate the influence of chain length on the rate of hydrolysis. For cellobiose (G2) hydrolysis, 46% conversion was achieved after 120 min of reaction (Fig. 1a). The hydrolysis pathway of cellobiose is shown in Scheme 1 and all steps were assumed to be first order reaction for kinetic analysis.[5,32] Accordingly, eqn (1)–(4) were used to represent the hydrolysis of cellobiose and degradation of glucose:

$$\frac{d[G2]}{dt} = -k_2\,[G2] \tag{1}$$

$$[G2] = [G2]_0 e^{-k_2 t} \tag{2}$$

$$\frac{d[Glucose]}{dt} = -k_1\,[Glucose] + 2k_2\,[G2] \tag{3}$$

$$[Glucose] = \frac{2k_2[G2]_0}{k_1 - k_2}\left(e^{-k_2 t} - e^{-k_1 t}\right) \tag{4}$$

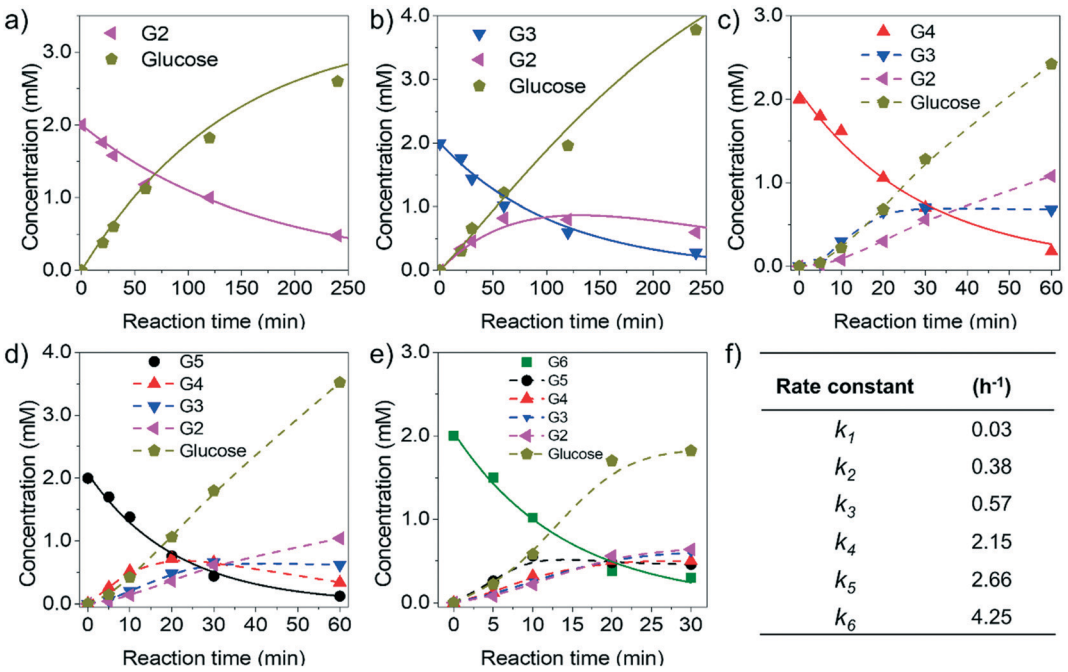

Fig. 1 Time-dependent conversion of oligosaccharides and evolution of products in the presence of AC-air: a) G2, b) G3, c) G4, d) G5, and e) G6. f) Rate constant for the hydrolysis of each cello-oligosaccharide. Reaction conditions: 1 μmol cello-oligosaccharides (G2–G6), 5 mg AC-air, 0.5 mL H_2O, 0.5 MPa Ar, 413 K. The symbols denote the experimental data points. The solid lines represent the simulation of reaction using the calculated rate constant and corresponding equations. The dashed lines show the experimental trend for the concentration of products during the reaction.

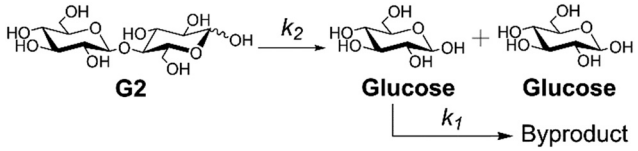

Scheme 1 Reaction pathway during hydrolysis of cellobiose.

where [G2] and [Glucose] are the concentrations of the respective compounds, $[G2]_0$ is the initial concentration of cellobiose, t is the reaction time, and k is the rate constant. The rate constant k_2 for the hydrolysis of cellobiose was determined to be 0.38 h^{-1} (Fig. 1f) by simulating eqn (2) to fit the experimental data. Similarly, the rate constant for the degradation of glucose (k_1) to other products was calculated to be 0.03 h^{-1}. The high k_2/k_1 ratio indicated that the decomposition of glucose under the reaction conditions was limited.

Hydrolysis of cellotriose (G3) under the same reaction conditions was faster than that of cellobiose and 50% conversion was achieved in 60 min. The hydrolysis of cellotriose to cellobiose and its further hydrolysis to glucose is shown in Scheme 2. The degradation of glucose to by-products was ignored owing to the very low value of k_1 estimated previously. Therefore, the hydrolysis rate constant k_3 was evaluated by the following rate eqn (5) and (6).

$$\frac{d[G3]}{dt} = -k_3\,[G3] \tag{5}$$

$$[G3] = [G3]_0 e^{-k_3 t} \tag{6}$$

The rate constant k_3 for the hydrolysis of cellotriose was calculated to be 0.57 h^{-1}. The simulation of the reaction profile by eqn (6), (8) and (10) along with the values of k_2 and k_3 fitted well with the experimental data (Fig. 1b).

$$\frac{d[G2]}{dt} = -k_2\,[G2] + k_3\,[G3] \tag{7}$$

$$[G2] = \frac{k_3[G3]_0}{k_2 - k_3}\left(e^{-k_3 t} - e^{-k_2 t}\right) \tag{8}$$

$$\frac{d[\text{Glucose}]}{dt} = 2k_2[G2] + k_3[G3] \tag{9}$$

$$[\text{Glucose}] = [G3]_0\left\{\frac{(k_3 - 3k_2)e^{-k_3 t} + 2k_3 e^{-k_2 t}}{k_2 - k_3} + 3\right\} \tag{10}$$

Based on the good fit of the rate equations for G2 and G3, the rate equation for the hydrolysis of cello-oligosaccharides was generalized:

$$\frac{d[Gx]}{dt} = -k_x\,[Gx] \tag{11}$$

$$[Gx] = [Gx]_0 e^{-k_x t} \tag{12}$$

where Gx represents the cello-oligosaccharide with a DP of x and k_x represents the rate constant for the hydrolysis of that cello-oligosaccharide.

The hydrolysis of cellotetraose (G4) was even faster (Fig. 1c) and k_4 was calculated to be 2.15 h^{-1}. Furthermore, the rate constants for the hydrolysis of cellopentaose (G5) and cellohexaose (G6) were calculated to be 2.66 h^{-1} and 4.25 h^{-1}, respectively (Fig. 1d and e). Consequently, kinetic analysis reveals that the rate of hydrolysis of cello-oligosaccharides increases dramatically with respect to their DP.

To ascertain if the increase in the rate of hydrolysis is caused by a favorable interaction between the cello-oligosaccharides and carbon catalyst or it is an inherent property of cello-oligosaccharides, we performed the hydrolysis of these compounds over other heterogeneous catalysts (Fig. 2). The time course for the hydrolysis of cello-oligosaccharides over Amberlyst 70 is shown in Fig. S3.† The rate constant for the hydrolysis of cellobiose on Amberlyst 70 was much higher (1.05 h^{-1}) in comparison to that on AC-air (0.38 h^{-1}) owing to its higher abundance of acid sites along with the high acid strength of the –SO_3H groups. However, unlike AC-air, the rate constant for the hydrolysis on Amberlyst 70 was not positively affected by an increase in DP. In contrast, the rate constant gradually decreased with an increase in the chain length of cello-oligosaccharides. H-Beta showed a significantly lower activity for the hydrolysis of cello-oligosaccharides (Fig. S4†) and the rate constant was not influenced by an increase in DP. The reaction rate in the presence of H-beta was not much different in comparison to that in a non-catalytic reaction (Fig. 2), suggesting the inability of H-beta zeolite to interact with cello-oligosaccharides.

We also evaluated the rate constant of cello-oligosaccharide hydrolysis in the presence of a homogeneous H_2SO_4 catalyst (Fig. S5†). The amount of H_2SO_4 used as a catalyst was adjusted to match the total number of acid sites when AC-air was used for the reaction. Hydrolysis in the presence of H_2SO_4 was much faster owing to its low pK_a and

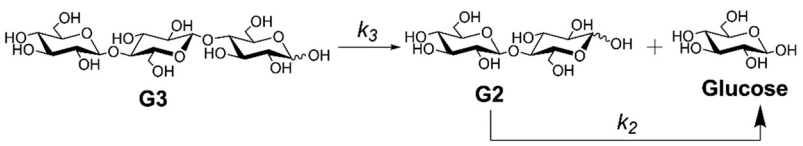

Scheme 2 Reaction pathway during hydrolysis of cellotriose.

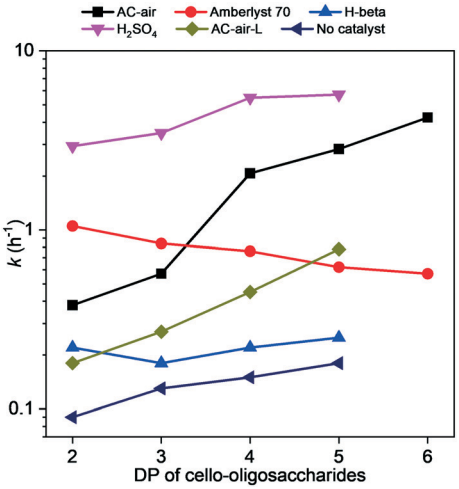

Fig. 2 Comparison of the change in the rate constant for the hydrolysis of cello-oligosaccharides in the presence of various acid catalysts. Reaction conditions: 1 μmol cello-oligosaccharides (G2–G6), 5 mg solid catalyst or 6.4 μmol H_2SO_4, 0.5 mL H_2O, 0.5 MPa Ar, 413 K.

homogeneous nature. The rate constant for the hydrolysis of cellobiose was 2.94 h^{-1}, a value 7.7 times higher than that for AC-air. A slight increase in the rate constant of hydrolysis over H_2SO_4 was also observed with increasing DP of cello-oligosaccharides. However, the change in the rate constant with DP was only 2.1 times from cellobiose to cellopentaose in comparison to 7 times for AC-air.

The rate of hydrolysis over AC-air-L was lower than that over AC-air for all the oligosaccharides due to the lower amount of functional groups on its surface. However, a similar increasing trend for the rate constant with DP of cello-oligosaccharides was obtained for AC-air-L. From these results, we conclude that carbon materials show a unique preferential interaction with cello-oligosaccharides and the increase in DP favors this interaction causing an increase in their rate of hydrolysis.

It can be argued that the hydrolysis rate increased due to the presence of more β-1,4-glycosidic linkages per molecule for larger cello-oligosaccharides. For example, cellobiose contains one glycosidic linkage whereas four linkages are present in cellopentaose. However, the rate constant increased 7 times from cellobiose to cellopentaose in the presence of AC-air, a value well above the increase in number of glycosidic linkages. Moreover, if the number of glycosidic linkages plays a crucial role, then its effect should be more prominent in the presence of H_2SO_4. However, the increase in rate constant was only 2.1 times in this case. This discrepancy further confirms the inherent ability of carbon catalysts to easily hydrolyze cello-oligosaccharides with a higher degree of polymerization.

Adsorption of cello-oligosaccharides over solid catalysts

One distinct property of carbon materials is their ability to adsorb carbohydrates, which is likely to influence the rate of hydrolysis. It has been clarified that the adsorption of β-1,4-glucans on the carbon surface occurs by CH–π and hydrophobic interactions.[26,28] Hydrolysis of cellulose is known to increase 13 times when it is adsorbed on a carbon surface by ball milling.[33] Therefore, we evaluated the adsorption of cello-oligosaccharides on all the catalysts in our study at room temperature to elucidate its influence on the rate of hydrolysis. Adsorption under the reaction conditions is expected to be lower than that at room temperature, but the change in adsorption capacity with respect to the cello-oligosaccharide size is expected to follow the same trend.[26]

H-Beta showed no adsorption of cello-oligosaccharides even though it had a relatively large surface area with a microporous structure. The same phenomenon was observed in the case of Amberlyst 70 and there was no difference in the concentration of cello-oligosaccharides during adsorption.

The adsorption of cello-oligosaccharides on AC-air was markedly different. The adsorption isotherms for G2–G5 oligosaccharides over AC-air are shown in Fig. 3a. They fitted well with the Langmuir adsorption model of type I isotherms in which the adsorption increased initially with the change in the concentration of the reactant and then plateaued once the adsorption capacity was reached.[26,28] Accordingly, the Langmuir formula shown in eqn (13) was used to calculate the adsorption capacity (Q_{max}) and adsorption equilibrium constant (K_{ads}):

$$\frac{C}{Q_e} = \frac{1}{Q_{max}} C + \frac{1}{K_{ads} Q_{max}} \quad (13)$$

where C is the equilibrium concentration of cello-oligosaccharides after adsorption, Q_e (mg $g_{adsorbent}^{-1}$) and Q_{max} (mg $g_{adsorbent}^{-1}$) are the adsorption amount and the maximum adsorption capacity of cello-oligosaccharides, respectively, and K_{ads} represents the adsorption equilibrium constant.

The Langmuir plots for each cello-oligosaccharide resulted in a good linear fit (Fig. 3b) and the calculated values for Q_{max} and K_{ads} are summarized in Table 2. The Q_{max} for cellobiose was 84 mg $g_{adsorbent}^{-1}$, which increased sequentially to 256 mg $g_{adsorbent}^{-1}$ for cellopentaose. Similarly, the K_{ads} value also increased 40-fold from G2 to G5. These parameters indicate that there is a stronger affinity for adsorption of larger cello-oligosaccharides on the carbon surface. AC-air-L showed higher Q_{max} and K_{ads} for all the cello-oligosaccharides in comparison to AC-air. AC-air-L is expected to have a higher polyaromatic surface area owing to the lower number of acidic functional groups and a larger surface area, which explains its higher adsorption capacity.

Fig. 3c shows a plot of the number of moles of oligosaccharides adsorbed over the carbon materials with respect to the DP under saturation adsorption conditions. For both carbon catalysts, the total molar adsorption of oligosaccharides was not influenced by the DP. Analysis of adsorption data reported by previous studies also shows that

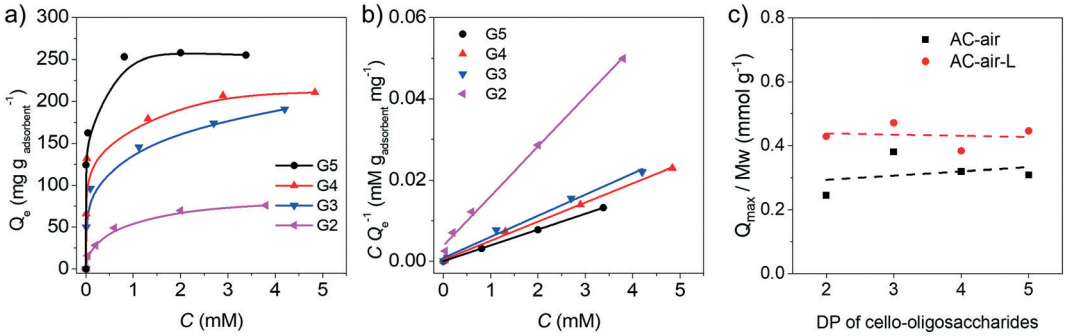

Fig. 3 Adsorption of cello-oligosaccharides (G2–G5) on AC-air: a) adsorption isotherms and b) Langmuir plot derived from eqn (13). c) Plot showing the maximum molar concentration of oligosaccharides over AC-air and AC-air-L at saturation.

equivalent molar adsorption occurs over other carbon materials. Over K26, an alkali activated carbon, the molar adsorption of cellobiose and cellotriose was calculated to be 1.2 and 1.0 mmol g^{-1}.[26] Similarly, over a mesoporous carbon surface, the molar adsorption for cellobiose, cellotriose and cellotetraose was calculated to be 1.6, 1.1 and 1.0 mmol g^{-1}.[28] Therefore, we conclude that although larger oligosaccharides show a higher affinity for adsorption over the carbon surface, this doesn't influence the surface concentration of oligosaccharides and this phenomenon is not linked with the type of carbon material used. Hence the increase in the rate of hydrolysis cannot simply be a result of higher abundance of larger oligosaccharides over the catalyst surface owing to stronger adsorption.

Affinity of cello-oligosaccharides and carbon catalysts

Adsorption can also influence the structure of large molecules, especially when they are adsorbed within narrow pores. To examine this possibility, we compared the microporous structure of the carbon materials with the size of cello-oligosaccharide molecules. The external surface area of AC-air calculated by the *t*-plot method was only 45 m^2 g^{-1}. AC-air-L had a similar structure with an external surface area of 55 m^2 g^{-1}. These surface areas are much lower than the minimum surface area required for adsorption of oligosaccharides under equilibrium conditions. This leads us to conclude that although adsorption may occur at any available surface area, the bulk of the cello-oligosaccharides is adsorbed within the micropores.

The pore size distribution of the carbon catalysts was determined by NLDFT simulation (Fig. 4). The AC-air and AC-air-L catalysts showed the presence of micropores smaller than 2.0 nm, with the peaks centered at 0.98 nm and 1.0 nm, respectively. Their pore width distributions became broader compared to that of pristine AC. In comparison, the cellobiose molecule has dimensions of 1.0 × 0.8 × 0.6 nm, whereas cellopentaose has dimensions of 2.5 × 0.7 × 0.6 nm. Therefore, the cello-oligosaccharides, especially the larger ones, must axially enter the micropores and adsorb within the micropores of the carbon catalysts.

The evolution of products during hydrolysis confirms this assertion. A closer inspection of hydrolysis data for cellotetraose (Fig. 5a) shows that the concentration of cellotriose was the same as glucose within the first 10 min of reaction, which was twice that of cellobiose. Preferential hydrolysis of terminal glycosidic bonds would cause a higher concentration of cellotriose and glucose (Fig. 5d). Axial adsorption of oligosaccharides would favor the hydrolysis of terminal glycosidic bonds. A similar trend was also observed in the cases of hydrolysis of cellopentaose (Fig. 5b) and cellohexaose (Fig. 5c), in which cellotetraose and cellopentaose appeared as primary products along with an equal amount of glucose. This observation is uniquely analogous to exoglucanase enzymes that sequentially cleave glucose or cellobiose molecules from the chain end of cellulose.[34] Hence we can claim that the notion of heterogeneous carbon catalysts randomly cleaving the β-1,4 glycosidic bonds of

Table 2 Langmuir constants of cello-oligosaccharide adsorption over the carbon catalysts at room temperature

	AC-air		AC-air-L	
Substrate	Q_{max} (mg g^{-1})	K_{ads} (M^{-1})	Q_{max} (mg g^{-1})	K_{ads} (M^{-1})
G2	84	2429	147	4000
G3	192	6500	238	42 000
G4	213	15 667	256	195 000
G5	256	97 500	370	—

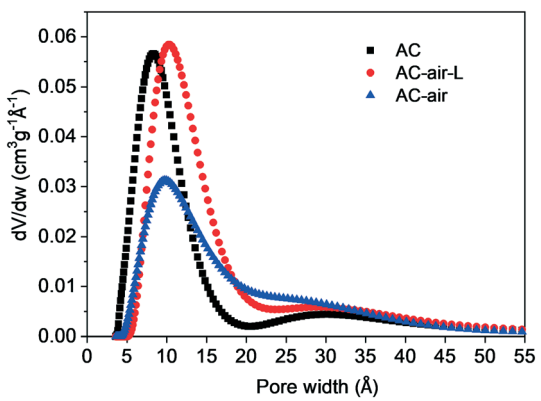

Fig. 4 Pore size distributions of the pristine and oxidized carbon catalysts determined by NLDFT simulation of N_2 adsorption isotherms.

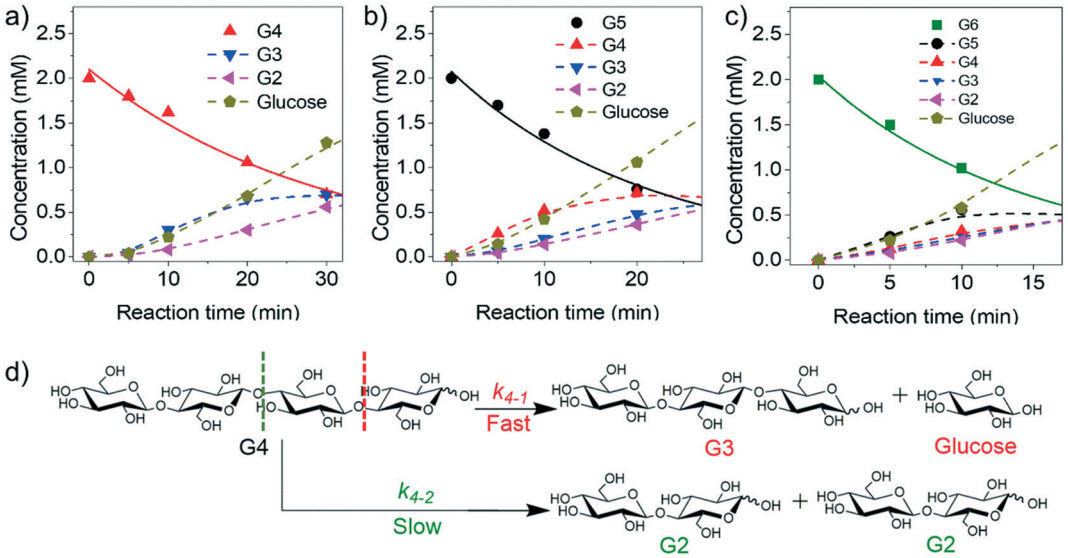

Fig. 5 Close-up of the reaction profiles shown in Fig. 1 to illustrate the evolution of products from a) G4 to b) G5 and c) G6 over the AC-air catalyst. d) Scheme showing the pathway for the hydrolysis of either the terminal glycosidic linkages or the internal glycosidic linkage in G4.

adsorbed cellulose molecules, in a manner analogous to endoglucanase, is not entirely true.

Activation energy of cello-oligosaccharides

Nevertheless, the axial adsorption and sequential cleavage of oligosaccharides also do not fully explain the increase in the rate of hydrolysis. So we evaluated the change in apparent activation energy during the hydrolysis of cello-oligosaccharides over AC-air. The Arrhenius equation for the calculation is shown in eqn (14):

$$\ln k = -\frac{E_a}{R}\frac{1}{T} + \ln A \quad (14)$$

where k (h^{-1}) is the rate constant of cello-oligosaccharide hydrolysis, E_a (kJ mol^{-1}) represents the activation energy for cello-oligosaccharide hydrolysis, A (h^{-1}) and T (K) are the pre-exponential factor for the reaction and the absolute reaction temperature, respectively, and R (kJ K^{-1} mol^{-1}) is the universal gas constant.

Hydrolysis of cello-oligosaccharides at other temperatures also conformed to the pattern of increase in rate constant with the increase in number of glycosidic bonds (Table 3 and Fig. S6–8†). The Arrhenius plots of these data fitted linearly with a high correlation coefficient (0.99, Fig. 6). The apparent activation energy for cellobiose hydrolysis was calculated to be 100 kJ mol^{-1}. A similar value of activation energy for cellotriose was obtained to be 98 kJ mol^{-1}. The activation energy for the hydrolysis of cellotetraose was 87 kJ mol^{-1} which further decreased to 77 kJ mol^{-1} for cellopentaose. This drastic reduction in the activation energy suggests a decrease in the energy required to cleave the glycosidic bonds as the DP increases. Furthermore, it might be expected that the stronger adsorption of larger oligosaccharides would lead to an increase in the pre-exponential factor (A). Instead, the value of A decreased, which could be attributed to the compensation effect observed when comparing E_a and A for reactions under similar conditions.[35]

Moreover, we further calculated the activation energy under the same reaction conditions in the presence of the H_2SO_4 catalyst (Fig. S9–S11†). The Arrhenius plots and the calculated values of activation energy are shown in Fig. S12.† An identical value of 100 kJ mol^{-1} for the activation energy of cellobiose hydrolysis was observed.‡ A slight decrease in activation energy was also detected with the increase of DP of cello-oligosaccharides. However, the activation energy decreased only by 11 kJ mol^{-1} from cellobiose to cellopentaose for H_2SO_4.

Proposed hydrolysis mechanism

Based on the above observations and in light of previous reports, we propose that in addition to the presence of oxygenated functional groups, the adsorption and

‡ This result was lower than a previously reported value of 120–130 kJ mol^{-1} for cellobiose hydrolysis over concentrated H_2SO_4.[5] The lower concentration of cellobiose in our reaction mixture (2 mM) was the reason for this low value because an activation energy of 139 kJ mol^{-1} was obtained when 50 mM solution of cellobiose was used in our reaction.

Table 3 Rate constant of cello-oligosaccharide hydrolysis at varying temperatures over AC-air and the calculated activation energy of hydrolysis for respective compounds

Substrate	k (h^{-1}) 403 K	413 K	423 K	433 K	E_a (kJ mol^{-1})	A (h^{-1})
G2	0.17	0.38	0.72	1.38	100	1.74×10^{12}
G3	0.33	0.57	1.44	2.64	98	1.71×10^{12}
G4	0.81	2.15	3.37	5.13	87	2.16×10^{11}
G5	1.43	2.66	4.57	6.91	77	1.10×10^{10}

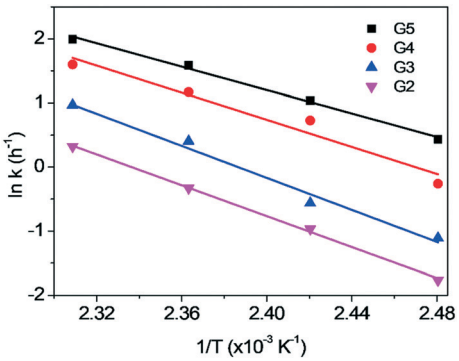

Fig. 6 Arrhenius plots of cello-oligosaccharide (G2–G5) hydrolysis on AC-air.

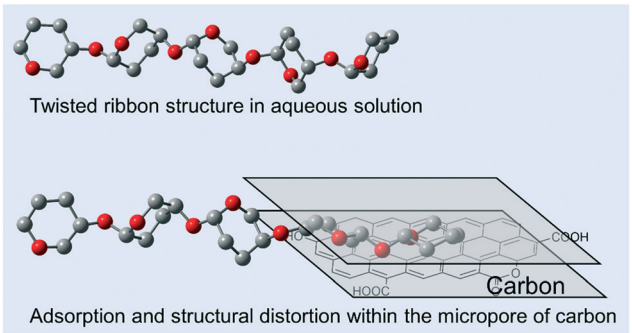

Fig. 7 Illustration showing the twisted ribbon structure of cellopentaose in water and the proposed structural change during the adsorption on the carbon surface. For clarity, the hydroxyl groups are not shown and only the pyranose rings linked by β-1,4-glycosidic bonds are depicted.

conformational change within the micropores influence the rate of hydrolysis of cello-oligosaccharides. The increase in the rate of hydrolysis with DP is caused by a decrease in activation energy required for hydrolysis of β-1,4-glycosidic bonds owing to their adsorption within the micropores of carbon. It is likely that the axial adsorption of a large molecule such as cellopentaose inside the micropores of carbon would cause a conformational change in its structure.[36] Cello-oligosaccharides conform to a stable twisted ribbon structure in aqueous solution.[37] Upon adsorption, this structure would untwist to accommodate itself within the pores and to achieve adsorption of multiple glucose units over the carbon surface (Fig. 7). This deviation from the stable twisted form could cause a change in the β-1,4-glycosidic bond angle, leading to reduction in activation energy required for its cleavage.

Conclusions

We performed hydrolysis of cello-oligosaccharides with increasing degree of polymerization in the presence of various catalysts. Only in the presence of carbon catalysts that the rate of hydrolysis was strongly dependent on the degree of polymerization. The hydrolysis rate constant increased 11 times with an increase in DP from 2 to 6. A simultaneous decrease in the apparent activation energy for hydrolysis was also observed with respect to the increase in DP. In addition, the larger oligosaccharides showed a stronger affinity towards adsorption over the narrow micropores of the carbon surface. A preference for hydrolysis of terminal over internal glycosidic bonds was observed, which was analogous to some enzymes in the cellulase family. Based on these observations, we propose that the increase in the rate of hydrolysis is caused by the reduction in activation energy which is the result of conformational changes in the oligosaccharide molecules when they adsorb within the micropores of carbon.

Conflicts of interest

There are no conflicts to declare.

Acknowledgements

This work was supported by the Japan Science and Technology Agency (JST) ALCA (JPMJAL1309). AS would like to acknowledge the funding support from the Research Fund Program for Early Career Scientists from Hokkaido University.

References

1 G. W. Huber, S. Iborra and A. Corma, *Chem. Rev.*, 2006, **106**, 4044–4098.
2 D. Klemm, B. Heublein, H.-P. Fink and A. Bohn, *Angew. Chem., Int. Ed.*, 2005, **44**, 3358–3393.
3 A. J. Ragauskas, C. K. Williams, B. H. Davison, G. Britovsek, J. Cairney, C. A. Eckert, W. J. Frederick, Jr., J. P. Hallett, D. J. Leak, C. L. Liotta, J. R. Mielenz, R. Murphy, R. Templer and T. Tschaplinski, *Science*, 2006, **311**, 484–489.
4 E. Kontturi, T. Tammelin and M. Osterberg, *Chem. Soc. Rev.*, 2006, **35**, 1287–1304.
5 R. Rinaldi and F. Schüth, *ChemSusChem*, 2009, **2**, 1096–1107.
6 H. Zhao, C. L. Jones, G. A. Baker, S. Xia, O. Olubajo and V. N. Person, *J. Biotechnol.*, 2009, **139**, 47–54.
7 N. Kamiya, Y. Matsushita, M. Hanaki, K. Nakashima, M. Narita, M. Goto and H. Takahashi, *Biotechnol. Lett.*, 2008, **30**, 1037–1040.
8 Q. Chu, X. Li, Y. Xu, Z. Wang, J. Huang, S. Yu and Q. Yong, *Process Biochem.*, 2014, **49**, 1217–1222.
9 A. T. To, P. W. Chung and A. Katz, *Angew. Chem., Int. Ed.*, 2015, **54**, 11050–11053.
10 Y.-B. Huang and Y. Fu, *Green Chem.*, 2013, **15**, 1095–1111.
11 S. Suganuma, K. Nakajima, M. Kitano, D. Yamaguchi, H. Kato, S. Hayashi and M. Hara, *J. Am. Chem. Soc.*, 2008, **130**, 12787–12793.
12 A. Charmot, P.-W. Chung and A. Katz, *ACS Sustainable Chem. Eng.*, 2014, **2**, 2866–2872.
13 A. Martin-Mingot, K. D. O. Vigier, F. Jérômeb and S. Thibaudeau, *Org. Biomol. Chem.*, 2012, **10**, 2521–2524.
14 T. Liebert, M. Seifert and T. Heinze, *Macromol. Symp.*, 2008, **262**, 140–149.

15 T. Hasunuma, K. Kawashima, H. Nakayama, T. Murakami, H. Kanagawa, T. Ishii, K. Akiyama, K. Yasuda, F. Terada and S. Kushibiki, *Anim. Sci. J.*, 2011, **82**, 543–548.
16 C. D. A. Souza, S. Li, A. Z. Lin, F. Boutrot, G. Grossmann, C. Zipfel and S. C. Somerville, *Plant Physiol.*, 2017, **173**, 2383–2398.
17 E. Billès, V. Coma, F. Peruch and S. Grelier, *Polym. Int.*, 2017, **66**, 1227–1236.
18 A. Shrotri, H. Kobayashi and A. Fukuoka, *Acc. Chem. Res.*, 2018, **51**, 761–768.
19 X. Zhang, K. Wilson and A. F. Lee, *Chem. Rev.*, 2016, **116**, 12328–12368.
20 A. Onda, T. Ochi and K. Yanagisawa, *Green Chem.*, 2008, **10**, 1033–1037.
21 B. R. Caes, M. J. Palte and R. T. Raines, *Chem. Sci.*, 2013, **4**, 196–199.
22 A. Shrotri, H. Kobayashi and A. Fukuoka, *ChemCatChem*, 2016, **8**, 1059–1064.
23 G. S. Foo and C. Sievers, *ChemSusChem*, 2015, **8**, 534–543.
24 H. Kobayashi, T. Komanoya, K. Hara and A. Fukuoka, *ChemSusChem*, 2010, **3**, 440–443.
25 A. Shrotri, H. Kobayashi and A. Fukuoka, *ChemSusChem*, 2016, **9**, 1299–1303.
26 M. Yabushita, H. Kobayashi, J.-Y. Hasegawa, K. Hara and A. Fukuoka, *ChemSusChem*, 2014, **7**, 1443–1450.
27 P. Dornath, S. Ruzycky, S. Pang, L. He, P. Dauenhauer and W. Fan, *Green Chem.*, 2016, **18**, 6637–6647.
28 P. W. Chung, A. Charmot, O. M. Gazit and A. Katz, *Langmuir*, 2012, **28**, 15222–15232.
29 P. Chen, A. Shrotri and A. Fukuoka, *ChemSusChem*, 2019, **12**, 2576–2580.
30 H. P. Boehm, *Carbon*, 2002, **40**, 145–149.
31 J. Guilera, R. Bringué, E. Ramírez, M. Iborra and J. Tejero, *Ind. Eng. Chem. Res.*, 2012, **51**, 16525–16530.
32 L. Vanoye, M. Fanselow, J. D. Holbrey, M. P. Atkins and K. R. Seddon, *Green Chem.*, 2009, **11**, 390.
33 M. Yabushita, H. Kobayashi, K. Hara and A. Fukuoka, *Catal. Sci. Technol.*, 2014, **4**, 2312–2317.
34 K. Igarashi, T. Uchihashi, A. Koivula, M. Wada, S. Kimura, T. Okamoto, M. Penttil, T. Ando and M. Samejima, *Science*, 2011, **33**, 1279–1282.
35 W. C. Conner Jr., *J. Catal.*, 1982, **78**, 238–246.
36 P.-W. Chung, M. Yabushita, A. T. To, Y. Bae, J. Jankolovits, H. Kobayashi, A. Fukuoka and A. Katz, *ACS Catal.*, 2015, **5**, 6422–6425.
37 M. Umemura, Y. Yuguchi and T. Hirotsu, *J. Phys. Chem. A*, 2004, **108**, 7063–7070.